

Direct real-space imaging of the $c(2 \times 8)/(2 \times 4)$ GaAs (001) surface structure

J. J. Kolodziej,^{1,*} M. Goryl,¹ J. Konior,¹ M. Reichling,² and M. Szymonski¹

¹Research Centre for Nanometer-Scale Science and Advanced Materials (NANOSAM), Faculty of Physics, Astronomy, and Applied Computer Science, Jagiellonian University, Reymonta 4, 30-059 Kraków, Poland

²Department of Physics, Osnabrück University, Barbarastrasse 7, 49076 Osnabrück, Germany

(Received 19 April 2007; revised manuscript received 27 August 2007; published 13 December 2007)

We have performed frequency-modulated atomic-force microscopy (FM-AFM) on the $c(2 \times 8)/(2 \times 4)$ GaAs (001) surface obtained from the $c(8 \times 2)/(4 \times 6)$ surface by exposing it to As_2 gas and annealing. Highly resolved interaction patterns reflect prevailing surface dimer pairs consistent with a so-called $\beta 2$ structure, but more rare motifs characteristic of $\alpha 2$ and β structures are also seen. Atoms of the dimers interact with the atomic force microscope tip repulsively and appear as sharp features on a smooth background when imaged in constant-height mode. An analysis of the interaction decay length and lateral size of the atomic features indicates that the surface atoms are visualized through a core-core repulsion mechanism. In this imaging mode, the FM-AFM can be regarded as a true surface structure tool, since the observed features are, in the absence of significant lateral relaxation, associated with surface atoms directly.

DOI: [10.1103/PhysRevB.76.245314](https://doi.org/10.1103/PhysRevB.76.245314)

PACS number(s): 68.35.Bs, 68.37.Ps, 68.47.Fg

I. INTRODUCTION

The GaAs (001) surface is an essential base for many heterostructures used today in optoelectronic and high-frequency electronic devices. This surface exhibits a number of reconstructions (surface phases) depending on stoichiometry of the top bilayer.¹ Among them, the arsenic rich $c(2 \times 8)/(2 \times 4)$ phase is the most relevant technologically and the most frequently studied, since it is a key for successful molecular beam epitaxy (MBE) growth of GaAs and, furthermore, a starting point for building useful devices. The structure was first obtained using MBE process and examined with reflected high-energy electron diffraction (RHEED) technique by Cho in the year 1971.² Later, to understand the structure, several models were discussed by Chadi³ and by Frankel *et al.*⁴ including “three-As-dimer” and “two-As-dimer” models, where the descriptive names refer to the number of As surface dimers in 2×4 structural subunits of that surfaces (later named as β and $\beta 2$, respectively). Although initially the “two-dimer” and the “three-dimer” structures were suggested to be almost degenerate in energy,^{3,5} some studies indicated the latter as the most likely one.⁶ Therefore, the interpretation of early scanning-tunneling microscopy (STM) images^{7,8} was given in terms of the three-dimer model. This interpretation was shortly after questioned by Falta *et al.*⁹ suggesting alternative Ga/As intermixing top layer structure, based on ion scattering data and by Northrup and Froyen,¹⁰ who indicated by total-energy calculations, that the two-dimer ($\beta 2$) structure is considerably lower in energy. Several theoretical papers followed with basically the same conclusion, i.e., indicating the two-dimer structure as the most stable one for standard MBE conditions.^{11–14} Strong support for the Chadi’s two-dimer model came also with x-ray diffraction study by Garreau *et al.*¹⁵

However, since MBE growth is a nonequilibrium process and structures far away from the global energy minimum are often kinetically accessible, words of explanation are due regarding other structures proposed for the surface under dis-

ussion. Based on RHEED patterns as fingerprints, Farell and Palmstrøm (FP)¹⁶ suggested three different phases α , β , and γ , ordered according to their increasing surface As content. According to FP, the unit of the α phase is constituted by two As dimers and dimerized Ga atoms in the second layer, the β phase is characterized by three As dimers as proposed by Chadi,³ and the γ phase is the β phase with additional As_2 dimers on top. However, further experimental studies using STM by Hashizume *et al.* evidenced that all α , β , and γ phases have the same unit structure in the top layer, comprising two-As-dimers and two-As-dimer vacancies. Therefore, Hashizume *et al.* proposed Chadi’s $\beta 2$ model for the β phase (coherently with theoretical results) and FP α model for the α phase. The γ phase was concluded to be a slightly disordered $\beta 2$ phase with some admixture of the $c(4 \times 4)$ phase.¹⁷ The last major revision has been suggested by Schmidt *et al.*¹⁸ who indicated that the $\alpha 2$ structure (introduced earlier by Yamaguchi and Horikoshi¹⁹ but not explored in depth) is significantly lower in energy than the α structure. This has been recently confirmed with independent calculations by Lee *et al.*²⁰

Although the structure of $c(2 \times 8)/(2 \times 4)$ reconstructed GaAs (001) surface has been extensively studied in the past, further studies from a different perspective, for example, using scanning force microscopy imaging, are valuable since for $A_{III}B_V$ surfaces, there are several recent examples where “well established” models have been questioned and dismissed.^{21,22} This point of view seems to be shared by a number of authors, as evidenced from many recent papers addressing this surface.^{23–28} In the present paper, we use frequency-modulated atomic-force microscopy (FM-AFM) in order to record characteristic interaction patterns for a number of different tip-surface distances in single experiment. This allows for separation of imaging-interaction components, analysis of their decay lengths, as well as for estimation of their spatial distributions. We identify the FM-AFM imaging mode possible in constant-height scanning, in which the imaging occurs through core-core repulsion mechanism. In this mode FM-AFM images directly re-

flect positions of protruding surface atoms as sharp repulsion points. We suggest that within this scheme, FM-AFM may be used as a technique for solving surface structure unambiguously.^{29,30} Eventually, we present the atomically resolved atomic-force microscopy (AFM) images of the $c(2 \times 8)/(2 \times 4)$ GaAs (001) surface, which allow for straightforward verification of structural models of this surface in real space.

II. EXPERIMENT

Experiments have been performed at the Jagiellonian University using an experimental system described in detail elsewhere.³¹ The sample is a piece of semi-insulating GaAs epi-ready wafer, mounted on a tantalum plate. The sample is outgassed overnight in vacuum at 850 K and then annealed in As_2 gas (1×10^{-6} mbar) at 950 K. Then, the temperature is lowered to 900 K and the sample is sputtered with an Ar^+ ion beam (see Ref. 31 for more details). As a result, the $c(8 \times 2)/(4 \times 6)$ surface is obtained. The $c(2 \times 8)/(2 \times 4)$ surface is obtained by exposing the sputter-cleaned surface to As_2 gas from a GaAs decomposition source (MBE-Komponenten) at 1×10^{-6} mbar during 1 min at room temperature (RT) and annealing the surface at 700 K during 1 h.

Scanning force microscopy is performed with a Park Scientific Instrument VP2 AFM/STM apparatus. All data are collected at RT. Force images are obtained in a frequency modulation mode with the use of a Nanosurf “easyPLL” demodulator. Commercially available piezoresistive silicon noncontact cantilevers are used as probes. The resonant frequencies (f_0) of cantilevers are 150–250 kHz and the spring constant is 20 N/m. The amplitude of cantilever oscillations used is 12 nm and detunings are below 100 Hz. The scanning rates are 1–3 Hz (see also Ref. 32). The tip is cleaned by heating at 1200 K during 30 s. Prior to measurements, the tip is crashed into the surface until a stable termination, having also atomic resolution capability, is reached. This is done during running image acquisition procedure, which allows for continuous monitoring of the tip quality and also for prompt withdrawing of the tip farther from surface when it acquires desired characteristics. By reasonable assumption, the imaging tip is in most cases terminated with gallium, arsenic, or silicon atom.

Two imaging (sub)modes are used. First is the topographic mode, when a feedback loop alternates the tip-surface distance, in order to maintain the constant frequency of the cantilever oscillation. In this case, a constant-frequency surface is measured. Second is a “quasi-constant-height” mode. In that case the feedback level is set rather low; consequently, the tip-surface distance is determined by averaging of interaction over many atomic sites and stays almost constant. In the result, a frequency shift (Δf) map is measured. Atomically resolved images are obtained at scanning rate of 3 Hz with residual feedback level tuned in such a way that the tip-surface distance is kept constant irrespective of thermal drifts and irrespective of slow (~ 1 Hz) mechanical instabilities of the experimental system. In the Δf maps presented here, brighter gray levels indicate lower cantilever oscillation frequencies (larger negative frequency

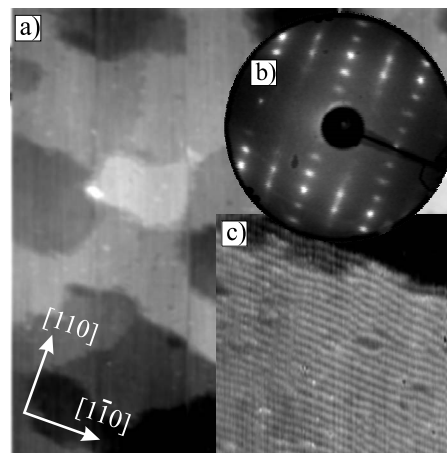


FIG. 1. (a) Topographic FM-AFM image ($0.5 \times 0.5 \mu\text{m}^2$) of GaAs $c(2 \times 8)/(2 \times 4)$ surface. (b) LEED pattern obtained at electron energy of 42 eV. (c) High resolution topographic image ($50 \times 50 \text{ nm}^2$) revealing stripes along $[1\bar{1}0]$ direction. All parts of the image are oriented according to the directions indicated by the white arrows.

shifts), indicating either more attractive or less repulsive interactions. It is expected that for atomically rough surfaces, imaged in the constant-height mode, only the most protruding atoms would be imaged since the short-range interactions, which may provide contrast on the atomic scale, vanish over lower parts of the structure.

III. RESULTS AND DISCUSSION

The structure of the as-prepared surface elucidated by AFM imaging and diffraction techniques is shown in Fig. 1. The surface is composed of large terraces separated by irregular bilayer steps [Fig. 1(a)]. The corresponding low-energy electron diffraction (LEED) pattern [Fig. 1(b)] evidences prevailing $c(2 \times 8)$ phase, however, with half-order spots streaking along $[110]$. Therefore, we prefer to use the $c(2 \times 8)/(2 \times 4)$ notation for the description of the phase. In Fig. 1(c), an intermediate scale structure is shown characterized by slightly meandering stripes that tend to be arranged parallel to the $[1\bar{1}0]$ direction. This AFM image is similar to the published STM images of MBE-prepared GaAs surfaces at this scale (see Refs. 33–35).

In Fig. 2, the structure of the top atomic layer is imaged with high resolution using the quasi-constant-height mode. The most striking characteristics of this FM-AFM pattern is that on smooth and uniform gray background sharp dark features, likely reflecting top layer atoms are imaged. The pattern indicates predominant double dimer rows (reminiscent of the $\beta 2$ structure) running along the $[1\bar{1}0]$ directions but with frequent kinks due to irregular shifts of the rows by one surface lattice basic unit (4 \AA) along $[110]$ (cf. Ref. 33). These shifts are responsible for visual meandering of the stripes seen in Fig. 1(c).

FM-AFM patterns reflect an oscillating cantilever frequency shift that arises due to complex mixture of tip-surface

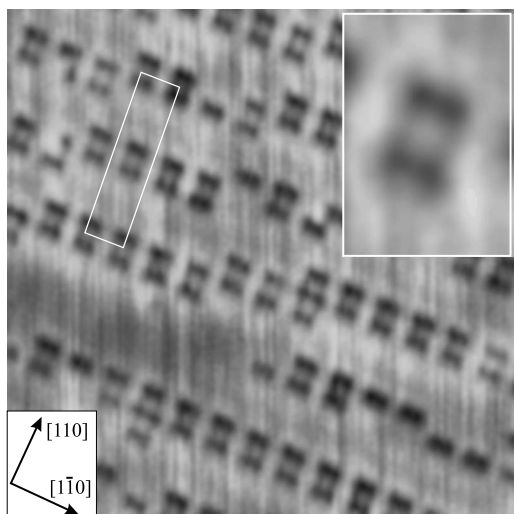


FIG. 2. FM-AFM image of $10 \times 10 \text{ nm}^2$ part of the surface shown in Fig. 1(c), quasiconstant-height mode, $\Delta f_{\text{aver}} = -24.5 \text{ Hz}$, and scanning rate is 3 Hz. The inset shows in magnification the double dimer detail. The white rectangle indicates the $c(2 \times 8)$ unit cell.

interactions.³⁶ These interactions include attractive and long-range macroscopic electrostatic interaction (capacitive forces), tip-surface polarization interaction (known also as van der Waals or vdW interaction) in a mesoscale, and short-range (chemical) interactions. Frequency shifts arising due to different interactions are small perturbations of the cantilever resonance frequency, and the total frequency shift is, to first order, the sum of the partial frequency shifts. During the FM-AFM imaging, the capacitive interaction is cancelled (with carefully tuned sample bias), while the mesoscale vdW interaction provides smooth attractive background. Crucial role in the imaging process plays the chemical interactions, which may be attractive or repulsive, *in principle*, and operate around oscillating cantilever lower turning point. They may be thought of, depending on the tip-surface system, as having electrostatic, covalent, metallic, or van der Waals nature, similarly to the chemical bond. It is obvious that the chemical interaction term is strongly dependent on the tip-front composition, structure, and charge state.

Since in the image of Fig. 2 large gray fields are present, where no atomic details can be seen, we may identify their gray tone with the mesoscale vdW background level (uniform over whole surface) that also denotes the zero level of the short-range interactions. Relative to this zero level, gray local attractive and repulsive short-range interactions are indicated by the brighter and the darker features, respectively.³⁷ The atomic-scale features in Fig. 2 are imaged as dark, which implies imaging through repulsive short-range interactions. The β_2 dimers are imaged with ultimate resolution; i.e., they are fully separated from each other, and moreover, atoms constituting the dimers are resolved [the dimer “necks” are visible (see the inset of Fig. 2)]. More rare, *single-dimer* (the most likely α_2) and three-dimer (β) structures and single adatoms are seen. In Table I, we present the dimensions of the observed structures and compare them

TABLE I. Characteristic distances for the observed surface structures. The distances are measured on a drift compensated map using the $c(2 \times 8)$ cell size as a reference.

	Distance (Å)	Std. error (Å)	Theor.
As-As (regular β_2 dimer)	2.51	0.10	2.50 ^a
As-As (kink β_2 dimer)	2.46	0.20	...
As-As (single α_2 dimer)	2.52	0.15	...
As-As (middle β dimer ^c)	3.65	...	2.50 ^a
As-As (side β dimer ^c)	2.50	...	2.50 ^a
dimer-dimer along [110] (β_2)	4.07	0.15	3.82 ^b

^aFrom Ref. 38 (DFT-LDA).

^bFrom Ref. 13 (DFT-LDA).

^cNo std. error, only two cases found with 3.60 and 3.70 Å separations.

to theoretical values found in literature. In overall, obtained microscopic data provide a direct view (this claim is discussed in detail further in the paper) of the $c(2 \times 8)/(2 \times 4)$ GaAs (001) top layer structure and evidences that the configurations identified previously as the lowest-energy ones, i.e., β_2 and α_2 are the most abundant, while others such as β are more rare and appear predominantly as structural irregularities. As seen from Table I, most As-As dimer lengths calculated using density functional theory and local density approximation (DFT-LDA) are consistent with our results; dramatic discrepancy is found, however, for the middle β dimer since its measured length is by 50% larger than the calculated one. The measured dimer-dimer separation along [110] is slightly larger than the one predicted by the DFT-LDA.

It is interesting to note that in the image of Fig. 2, atomic features have a width of only 2.2 Å (Gaussian full width at half maximum) which is, despite the apparatus broadening, even less than the arsenic double atomic radius (2.4 Å). Such a result indicates that the imaging mechanism is dominated by repulsive interactions of extremely short range. In order to verify this hypothesis, we scan the surface using the quasiconstant-height mode and gradually vary the average detuning by 1 Hz steps. At the end of the scan, we set initial detuning value to obtain data for linear correction of the vertical drift. The atomically resolved image is recorded in the Δf channel [see Fig. 3(a)], while the topographic channel provides an image of steps reflecting the tip height over the scanned surface [Fig. 3(b)]. At this point, it is important to understand sources and character of the noise present in our microscope signals. A rigid experimental setup is isolated from ground noise by pneumatic legs, and the whole system has base resonant vibration frequency of $\sim 1 \text{ Hz}$. The frequencies significantly higher than 1 Hz are not transmitted through the legs. On the other hand, the scan frequency is 3 Hz, and single lines of the high resolution images shown here are acquired during the time less than one-sixth of a second (since forth and back scan images are acquired simultaneously). Therefore, the image frequencies reflecting atomic patterns are well separated from the noise frequencies. Additionally, the tip-surface distance is controlled by

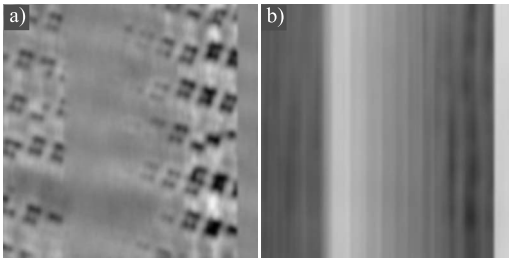


FIG. 3. (a) Δf image recorded with detuning set initially to -24.5 Hz (slow scan direction is from left to right), then gradually varied by 1 Hz steps from -17.5 Hz to -26.5 Hz, and shortly before the end it is set back to 17.5 Hz, $f_0=250$ kHz. (b) Corresponding topographic channel.

the Δf signal dominated by the mesoscale vdW interaction not depending on the scanner position in plane. As a result, in the quasiconstant-height mode, the scanner trajectory does not diverge far from the ideal constant-height trajectory. Moreover, in this mode, the oscillatory signal corresponding to bending of the microscope stage, following slow (1 Hz) rocking movement of the whole system, is present in the topographic channel only but not in the Δf channel. This oscillatory noise is easily removed by averaging of the step levels. The height (z position) of the scanner, during the variable Δf scan, is presented in Fig. 4(a) and the higher-frequency residuals, giving the measure of an error caused by the use of quasiconstant-height mode, are shown in Fig. 4(b). As the uncertainty in the tip height over surface (z), we take the maximal observed deviation, i.e., ± 0.01 nm. For different z values (or steps), we analyze the sections of the Δf image over crystallographically equivalent surface atoms (black

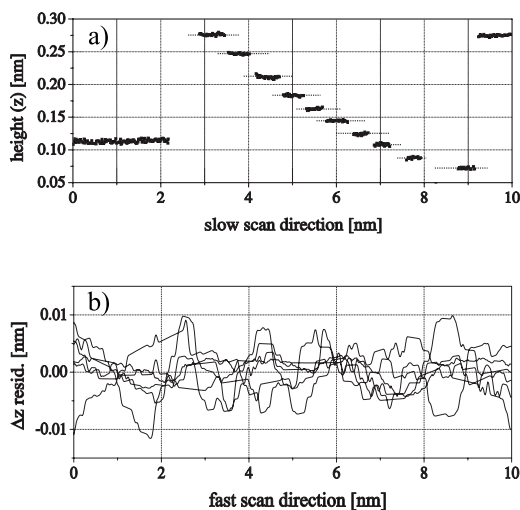


FIG. 4. (a) Tip heights over surface obtained from Fig. 3(b) by averaging along and across the scan lines. Parts corresponding to not stationary conditions (occurring due for setting of different discrete detuning levels) are omitted for clarity. The heights have been corrected for the scanner vertical drift. (b) Six quasiconstant-height residuals (including two lines recorded at extreme detuning of -26.5 Hz) illustrating the divergence of actual tip trajectories above surface from ideal constant-height ones.

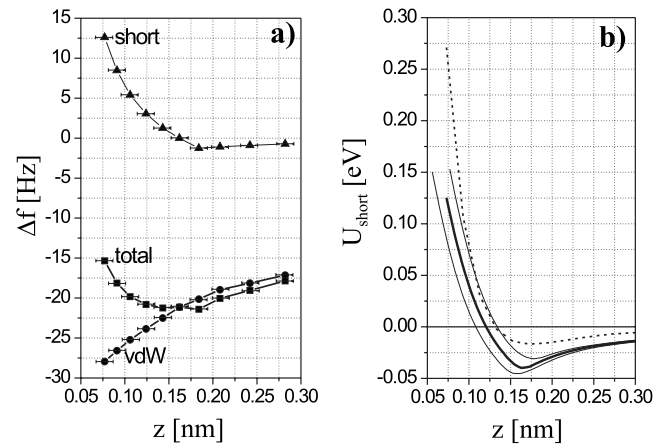


FIG. 5. (a) FM-AFM interaction curves over As top layer atoms obtained from the Δf image recorded with detuning gradually varied by 1 Hz steps from -17.5 to -26.5 Hz, $f_0=250$ kHz. The “total” curve is the sum of “van der Waals” and short curves. (b) Potential of the short-range tip-surface interaction obtained from the short Δf curve—solid line. Error limits calculated assuming ± 0.01 nm z uncertainty are indicated by thin solid lines. Systematic spring constant (k) error is estimated as 20% (not included in the error limits in the figure). Krypton-krypton interaction potential from Ref. 40 shown for reference—dotted line (krypton is the noble gas element close to As in the periodic table). The z -scale zero is arbitrary.

features) and we determine the frequency shift arising due to the short-range interactions, i.e., the difference in frequency between the vdW background level (away from the atomic features) and the maximum of the feature reflecting the surface atom. For all steps, we also read, on the Δf map, the difference between the average level and the vdW background level and combine it with the average detuning value to determine frequency shift related to the mesoscale vdW interaction. Such a procedure allows us to avoid two serious flaws associated with standard site-specific force spectroscopy when the tip is brought over specified point on the previously measured surface map and the Δf dependence as a function of z is measured in a single step. The first flaw is associated with uncertainty of the lateral tip position at the spectroscopy point both due to thermal drifts and due to the fact that for given surface point, its dynamic (during imaging) and static (during spectroscopy) coordinates, in terms of steering piezovoltages, often differ significantly. The second flaw is associated with uncertain separation of vdW interaction and the short-range interactions done on the basis of single curve by the extrapolation of the vdW curve to short ranges while the fit is done to its far tail.

Our evaluated interaction curves are shown in Fig. 5. The short-range part on the tip-surface interaction energy $U_{\text{short}}(z)$, calculated from the “short” Δf interaction curve of Fig. 5(a) using the Sader-Jarvis algorithm,³⁹ is presented in Fig. 5(b). In order to implement the Sader-Jarvis algorithm, the interaction tail has been test fitted with several functions having different asymptotic behaviors for large z . It has been concluded that the shape of the tail has no effect on the inverted potential within the short range apart from meaning-

less vertical shifts of the whole potential curve within this range. The potential $U_{\text{short}}(z)$ has a slightly attractive tail, but the attractive energy is only of the order of the room temperature kT . This attractive interaction has rather large spatial extent as concluded from bright “halo” around the double dimer, shown as the inset of Fig. 2, as well as from the lack of sharp atomic details within the pure attractive interaction range. Since the decay characteristics of this weak attractive interaction and of the krypton-krypton attractive tail are similar, we think that this attraction is due to microscopic van der Waals interactions, i.e., polarization interactions of the tip-front atom and several close surface dimers. The $U_{\text{short}}(z)$ potential is rather steep in its repulsive part and, in fact, it is comparable with a Kr-Kr interatomic potential [Fig. 5(b)]. Thus, we come to the conclusion that the interactions giving dark atomically resolved patterns are related to a core-core repulsion onset. Since the core-core interactions are concentrated around atomic nucleus and have a symmetry close to the circular one, our “dark” imaging mode gives in-plane coordinates of protruding surface atoms directly. On the bases of Fig. 3(a), we exclude significant lateral relaxation following the pressure exerted by the tip on surface atoms, since no variation of surface geometry, no discontinuities, and no loss of resolution is seen upon imaging with increased detuning. This is in contrast to significant relaxation observed for “soft” structures, for example, Si(001) $c(4 \times 2)$ phase.⁴¹ However, while the latter exists only at kriogenic temperatures, the $c(2 \times 8)/(2 \times 4)$ GaAs phase is thermally stable up to 700 K, while the maximal interaction energy observed in present experiment is about 0.1 eV. This interaction energy does not seem to be excessively large when compared with GaAs surface atom displacement energy that has to be of the order of a few electron volts. It is also interesting to note that we do not see the formation of strong chemical bonds between the tip and the surface As dimers but only weak attractive interactions, likely having vdW nature. Therefore, the tip-front atom is probably a passivated arsenic atom. Accordingly, we have used the Kr-Kr interaction potential as a reference, since it should roughly model the passivated As-As repulsion due to similarities in the electronic structure of those elements.

Our images recorded using the FM-AFM technique allow for an unambiguous, atomically resolved identification of the $c(2 \times 8)/(2 \times 4)$ GaAs (001) surface structure in real space.

This is in contrast to many published atomically resolved STM images of this surface (for examples, see Refs. 7, 8, 17, 19, 25, 26, and 28), which show as a rule to the only fuzzy rectangles reflecting (2×4) structural subunits. A few higher resolution studies available^{33,42–45} show some weak subunit structure, but individual dimers and atoms are not resolved.⁴⁶ This indicates that an unambiguous interpretation of STM patterns for the surface under study would require full theoretical modeling, which is, in fact, not possible without the detailed knowledge about the structure of the scanning tip.

IV. CONCLUSIONS

In conclusion, we have studied the $c(2 \times 8)/(2 \times 4)$ reconstructed GaAs (001) surface using FM-AFM, and we have presented highly resolved images in real space. We have confirmed that this surface is predominantly composed of the structural motifs characteristic of $\beta 2$ and $\alpha 2$ phases. We have also found rare three-dimer (β) motifs which appear significantly different from their theoretical model.

We have achieved spectroscopic capability at room temperature. As evidenced by the imaging-interaction decay length, the surface As atoms are imaged at constant height by a core-core repulsion mechanism. FM-AFM becomes, that way, a true surface structure tool, since in this imaging mode, the positions of protruding surface atoms are simply equivalent to the positions of dark spots in the repulsive FM-AFM interaction patterns. Of course, the absence of significant lateral relaxation must be observed simultaneously, but we think that signatures of such relaxation are identifiable in the experimental noncontact-AFM patterns.

After having many compound semiconductor surfaces imaged by FM-AFM,³² we are convinced that the repulsive imaging mode described here is not exotic; conversely, for some structures (including the one studied here), it is even the most frequently achieved high-resolution FM-AFM imaging mode at constant height.

ACKNOWLEDGMENTS

This work has been supported by the European Commission under Contract No. MTKD-CT-2004-003132 and by the Polish Ministry of Education and Science under Grant No. 1P03B 067 26.

*Corresponding author. jkolodz@if.uj.edu.pl

¹P. Drathen, W. Ranke, and K. Jacobi, Surf. Sci. **77**, 162 (1978).

²A. Y. Cho, J. Appl. Phys. **42**, 2074 (1971).

³D. J. Chadi, J. Vac. Sci. Technol. A **5**, 834 (1987).

⁴D. J. Frankel, C. Yu, J. P. Harbison, and H. H. Farrell, J. Vac. Sci. Technol. B **5**, 113 (1987).

⁵J. E. Northrup and S. Froyen, Phys. Rev. Lett. **71**, 2276 (1993).

⁶P. K. Larsen and D. J. Chadi, Phys. Rev. B **37**, 8282 (1988).

⁷M. D. Pashley, K. W. Haberern, W. Friday, J. M. Woodall, and P. D. Kirchner, Phys. Rev. Lett. **60**, 2176 (1988).

⁸D. K. Biegelsen, R. D. Bringans, J. E. Northrup, and L. E. Swartz, Phys. Rev. B **41**, 5701 (1990).

⁹J. Falta, R. M. Tromp, M. Copel, G. D. Pettit, and P. D. Kirchner, Phys. Rev. Lett. **69**, 3068 (1992).

¹⁰J. E. Northrup and S. Froyen, Phys. Rev. B **50**, 2015 (1994).

¹¹N. Moll, A. Kley, E. Pehlke, and M. Scheffler, Phys. Rev. B **54**, 8844 (1996).

¹²S. B. Zhang and A. Zunger, Phys. Rev. B **53**, 1343 (1996).

¹³W. G. Schmidt and F. Bechstedt, Phys. Rev. B **54**, 16742 (1996).

¹⁴T. Ohno, Thin Solid Films **272**, 331 (1996).

- ¹⁵Y. Garreau, M. Sauvage-Simkin, N. Jedrecy, R. Pinchaux, and M. B. Veron, *Phys. Rev. B* **54**, 17638 (1996).
- ¹⁶H. H. Farrell and C. J. Palmström, *J. Vac. Sci. Technol. B* **8**, 903 (1990).
- ¹⁷T. Hashizume, Q.-K. Xue, J. Zhou, A. Ichimiya, and T. Sakurai, *Phys. Rev. Lett.* **73**, 2208 (1994).
- ¹⁸W. G. Schmidt, S. Mirbt, and F. Bechstedt, *Phys. Rev. B* **62**, 8087 (2000).
- ¹⁹H. Yamaguchi and Y. Horikoshi, *Phys. Rev. B* **51**, 9836 (1995).
- ²⁰S.-H. Lee, W. Moritz, and M. Scheffler, *Phys. Rev. Lett.* **85**, 3890 (2000).
- ²¹C. Kumpf, L. D. Marks, D. Ellis, D. Smilgies, E. Landemark, M. Nielsen, R. Feidenhans'l, J. Zegenhagen, O. Bunk, J. H. Zeysing, Y. Su, and R. L. Johnson, *Phys. Rev. Lett.* **86**, 3586 (2001).
- ²²A. Ohtake, S. Tsukamoto, M. Pristovsek, N. Koguchi, and M. Ozeki, *Phys. Rev. B* **65**, 233311 (2002).
- ²³A. Balzarotti, E. Placidi, F. Arciprete, M. Fanfoni, and F. Patella, *Phys. Rev. B* **67**, 115332 (2003).
- ²⁴A. Ohtake, M. Ozeki, T. Yasuda, and T. Hanada, *Phys. Rev. B* **65**, 165315 (2002).
- ²⁵P. Laukkanen, M. Kuzmin, R. E. Perala, M. Ahola, S. Mattila, I. J. Vayrynen, J. Sadowski, J. Konttinen, T. Jouhti, C. S. Peng, M. Saarinen, and M. Pessa, *Phys. Rev. B* **72**, 045321 (2005).
- ²⁶D. W. Pashley, J. H. Neave, and B. A. Joyce, *Surf. Sci.* **582**, 189 (2005).
- ²⁷F. Arciprete, C. Goletti, E. Placidi, C. Hogan, P. Chiaradia, M. Fanfoni, F. Patella, and A. Balzarotti, *Phys. Rev. B* **69**, 081308(R) (2004).
- ²⁸M. J. Hale, S. I. Yi, J. Z. Sexton, and A. C. Kummel, *J. Chem. Phys.* **119**, 6719 (2003).
- ²⁹M. A. van Hove, *Prog. Surf. Sci.* **64**, 157 (2000).
- ³⁰M. A. van Hove, *Surf. Interface Anal.* **28**, 36 (1999).
- ³¹J. J. Kolodziej, B. Such, and M. Szymonski, *Phys. Rev. B* **71**, 165419 (2005).
- ³²J. J. Kolodziej, B. Such, M. Goryl, F. Krok, P. Piatkowski, and M. Szymonski, *Appl. Surf. Sci.* **252**, 7614 (2006).
- ³³A. R. Avery, C. M. Goringe, D. M. Holmes, J. L. Sudijono, and T. S. Jones, *Phys. Rev. Lett.* **76**, 3344 (1996).
- ³⁴M. Itoh, *Prog. Surf. Sci.* **66**, 53 (2001).
- ³⁵U. Resch-Esser, N. Esser, C. Springer, J. Zegenhagen, W. Richter, M. Cardona, and B. O. Fimland, *J. Vac. Sci. Technol. B* **13**, 1672 (1995).
- ³⁶M. Guggisberg, M. Bammerlin, Ch. Loppacher, O. Pfeiffer, A. Abdurixit, V. Barwich, R. Bennewitz, A. Baratoff, E. Meyer, and H.-J. Guntherodt, *Phys. Rev. B* **61**, 11151 (2000).
- ³⁷We display our maps with Δf increasing from bright to dark.
- ³⁸W. G. Schmidt, *Appl. Phys. A: Mater. Sci. Process.* **65**, 581 (1997).
- ³⁹J. E. Sader and S. P. Jarvis, *Appl. Phys. Lett.* **84**, 1801 (2004).
- ⁴⁰R. A. Aziz, *Mol. Phys.* **38**, 177 (1979).
- ⁴¹Y. J. Li, H. Nomura, N. Ozaki, Y. Naitoh, M. Kageshima, Y. Sugawara, C. Hobbs, and L. Kantorovich, *Phys. Rev. Lett.* **96**, 106104 (2006).
- ⁴²V. P. LaBella, H. Yang, D. W. Bullock, P. M. Thibado, P. Kratzer, and M. Scheffler, *Phys. Rev. Lett.* **83**, 2989 (1999).
- ⁴³L. D. Broekman, R. C. G. Leckey, J. D. Riley, A. Stampfl, B. F. Usher, and B. A. Sexton, *Phys. Rev. B* **51**, 17795 (1995).
- ⁴⁴V. Bressler-Hill, M. Wassermeier, K. Pond, R. Maboudian, G. A. D. Briggs, P. M. Petroff, and W. H. Weinberg, *J. Vac. Sci. Technol. B* **10**, 1881 (1992).
- ⁴⁵U. Resch Esser, N. Esser, D. T. Wang, M. Kuball, J. Zegenhagen, B. O. Fimland, and W. Richter, *Surf. Sci.* **352**, 71 (1996).
- ⁴⁶In Ref. 44 three-dimer structure is shown. We think that this may be experimental artifact. During our experiments, we have often seen false three-dimer structures. The pattern could be switched to two dimer by a soft crash. Therefore we think that malicious tip configurations are not unlikely when using scanning-probe techniques, and here, we present low symmetry image, i.e., with many kinks, defects, and single adatoms to avoid this risk.